

Simulating the transport and dispersal of volcanic ash clouds with initial conditions created by a 3D plume model

Zhixuan Cao^{1,2} Marcus Bursik³ Qingyuan Yang^{4,5} Abani Patra^{*,1,6}

¹ Mechanical and Aerospace Engineering Department, SUNY Buffalo, Buffalo, NY, USA

² Fluids Business Unit, ANSYS Inc, Lebanon, NH, USA

³ Center for Geohazards Studies, SUNY Buffalo, Buffalo, NY, USA

⁴ Earth Observatory of Singapore, Singapore, Singapore

⁵ The Asian School of the Environment, Nanyang Technological University, Singapore, Singapore

⁶ Data Intensive Studies Center, Tufts University, Medford, MA, USA

Correspondence*:

Abani Patra

abani.patra@tufts.edu

2 ABSTRACT

3 VATD (volcanic ash transport and dispersion) models simulate atmospheric transport of ash
4 starting from a source originating at the volcano represented by concentration of ash with height.
5 Most VATD models use a source of some prescribed shape calibrated against an empirical
6 expression for the height-mass eruption rate (MER) relation. The actual vertical ash distribution
7 in volcanic plumes usually varies from case to case and have complex dependencies on eruption
8 source parameters and atmospheric conditions. We present here for the first time the use of a
9 3D (three-dimensional) plume model to represent the ash cloud source without any assumption
10 regarding plume geometry. By eliminating assumed behavior associated with a semi-empirical
11 plume geometry, the predictive skill of VATD simulations is greatly improved. To date, no VATD
12 simulation adopts initial conditions created from first principles based on a 3D plume simulation.
13 We use our recently developed volcanic plume model based on a 3D smoothed-particle hydrody-
14 namic Lagrangian method, and couple the output to a standard Lagrangian VATD model. We
15 apply the coupled model to historical eruptions to illustrate the effectiveness of the approach.
16 Our investigation reveals that initial particle distribution in the vertical direction has more impact
17 on transport of ash clouds than does the horizontal distribution. Comparison with satellite data
18 indicates that ash particles are concentrated through the depth of the volcanic umbrella cloud,
19 and much lower than observed maximum plume height.

20 **Keywords:** VATD, volcano, 3D plume model, initial conditions, numerical simulation, SPH, Pinatubo, ash transport, ash dispersal

1 INTRODUCTION

21 Volcanic ash, the fine-grained fraction of tephra can be widely dispersed to synoptic and global scales, and
22 can lead to a degradation of air quality and pose threats to aviation (Tupper et al., 2007). Identification,
23 tracking and modeling the future movement of volcanic ash help route and schedule flights to avoid ash

24 clouds. Numerical estimation of ash distribution using known and forecast wind fields is necessary if we
25 are to accurately predict ash cloud propagation and spread. Numerous VATD (volcanic ash transport and
26 dispersion) models have been developed by both civil and military aviation, and meteorological agencies to
27 provide forecasts of ash cloud motion (Witham et al., 2007). New techniques have been integrated into
28 VATDs to satisfy increasing demands for different types of output, model accuracy and forecast reliability.
29 This contribution explores a method for creating initial conditions for VATD simulations, which promises
30 to improve prediction capability.

31 Fero et al. (2009) and Stohl et al. (2011) showed that initial source conditions have significant effects on
32 simulation of volcanic ash transport. Traditional VATD simulation requires key global descriptors of the
33 volcanic plume, especially plume height, grain size, eruption duration and mass loading, or alternatively, a
34 mass eruption rate (MER). No matter how these global descriptors are obtained, they are used to furnish the
35 initial conditions for VATDs in the form of a line-source term of a spatio-temporal distribution of particle
36 mass. It is a common practice to pick values for these global descriptors using an empirical expression for
37 the height-MER relation. The empirical expression is written as a function of several parameters, including
38 the key global descriptors. The values for the descriptors can also be found by parameter calibration (e.g.
39 Fero et al., 2008, 2009; Stohl et al., 2011; Zidikheri et al., 2017). One-dimensional (1D) plume models
40 serve as an alternative option to provide values. For example, Bursik et al. (2012) used the 1D model puffin
41 (Bursik, 2001) to generate estimates of mass eruption rate and grain size. In some cases, an extra step is
42 adopted to spread ash particles from the line source horizontally, resulting in an initial ash cloud in 3D
43 space. The horizontal spreading depends on an empirical expression. For example, the VATD model Puff
44 spreads particles from the line source uniformly in the horizontal direction within a given radius using
45 an empirical expression generated from the output of puffin. Considering the complexities of volcanic
46 eruptions, the actual ash distribution in the initial ash cloud should vary from case to case and with time,
47 making it difficult to find one general expression that is suitable for all cases. It is useful therefore to
48 investigate alternative ways for creating initial ash clouds without assumptions regarding plume geometry,
49 or numerical inversion. This provides the major motivation of this paper.

50 VATD models can be categorized into Lagrangian particle tracking and Eulerian advection-diffusion
51 types. Among several available particle tracking models (e.g. Walko et al., 1995; Searcy et al., 1998;
52 D'amours, 1998; Draxler and Hess, 1998) and advection-diffusion models (e.g. Bonadonna and Houghton,
53 2005; Folch et al., 2009; Schwaiger et al., 2012), we adopt a particle tracking model, Puff (Tanaka, 1991;
54 Searcy et al., 1998), as the primary VATD model. Puff can accept a 3D point cloud description of the
55 starting ash cloud as an initial condition, which makes it technically easier to couple with 3D plume models.
56 Puff initializes a discrete number of tracers that represent a sample of the eruption cloud, and calculates
57 transport, turbulent dispersion, and fallout for each representative tracer. A cylinder emanating vertically
58 from the volcano summit to a specified maximum height is the standard approach to provide a simple model
59 of the geometry of a typical ash column. Puff minimally requires horizontal wind field data. The “restart”
60 feature of Puff makes it technically feasible to accommodate the hand-off between a plume simulation and
61 the Puff simulation in terms of time and length scales.

62 We also implement one of the most widely used models for atmospheric trajectory and dispersion
63 calculations, the Hybrid Single-Particle Lagrangian Integrated Trajectory model (HYSPLIT) (Stein et al.,
64 2015; Rolph et al., 2017), developed by NOAA’s Air Resources Laboratory. HYSPLIT is able to simulate
65 phenomena from simple back trajectories, to very sophisticated computations of transport, mixing, chemical
66 transformation, and deposition of pollutants and hazardous materials. It is used in this study to better
67 understand simulation results from Puff.

68 Besides parameter calibration, 1D plume models have been used to obtain global descriptors of volcanic
69 plumes. 1D plume models (e.g. Woods, 1988; Bursik, 2001; Mastin, 2007; de'Michieli Vitturi et al., 2015;
70 Folch et al., 2016; Pouget et al., 2016) solve the equations of motion in 1D using simplifying assumptions,
71 and hence depend on estimation of certain parameters, especially those related to the entrainment of air,
72 which is evaluated based on two coefficients: a coefficient due to turbulence in the rising buoyant jet, and
73 one due to the crosswind field. Different 1D models adopt different entrainment coefficients based on a
74 specific formulation or calibration against well-documented case studies. The feedback from plume to
75 atmosphere is usually ignored in 1D models. While these 1D models generated well-matched results with
76 3D models for plumes that are dominated by wind (often called weak plumes) much greater variability
77 is observed for strong plume scenarios (Bursik et al., 2009; Costa et al., 2016). On the other hand, 3D
78 numerical models for volcanic plumes based on first principles and having few parametrized coefficients
79 (Oberhuber et al., 1998; Neri et al., 2003; Suzuki et al., 2005; Cerminara et al., 2016a; Cao et al., 2018)
80 naturally create a 3D ash cloud, which could serve directly as an initial state of the volcanic material for
81 VATDs. However, there is no VATD simulation using such 3D ash clouds as initial conditions. In this paper,
82 we will carry out VATD simulations using an initial state for the ash cloud based on 3D plume simulations,
83 generated with Plume-SPH (Cao et al., 2018, 2017). The implementation techniques described in this paper
84 can be applied to any combination of VATD model and 3D plume model even though our investigation is
85 based on a specific VATD model and plume model.

86 The 1991 eruption of Pinatubo volcano is used as a case study. Pinatubo erupted between June 12 and 16,
87 1991, after weeks of precursory activity. The climactic phase started on June 15 at 0441 UTC and ended
88 around 1341 UTC (Holasek et al., 1996a). The climactic phase generated voluminous pyroclastic flows,
89 and sent Plinian and co-ignimbrite ash and gas columns to great altitudes (Scott et al., 1996). The evolution
90 of the Pinatubo ash and SO_2 clouds was tracked using visible (Holasek et al., 1996a), ultraviolet (Total
91 Ozone Mapping Spectrometer; TOMS) (Guo et al., 2004a) and infrared sensors, including the Advanced
92 Very High-Resolution Radiometer (AVHRR) (Guo et al., 2004b). There is sufficient observational data to
93 estimate the eruption conditions for the climactic phase of the eruption (Suzuki and Koyaguchi, 2009). The
94 availability of calibrated eruption conditions and extensive observational data regarding ash cloud transport
95 make the Pinatubo eruption an ideal case study.

2 MATERIALS AND METHODS

96 2.1 Plume-SPH Model

97 Plume-SPH (Cao et al., 2018) is designed to describe an injection of well mixed solid and volcanic gas
98 from a circular vent above a flat surface into a stratified stationary atmosphere. The basic assumptions of
99 the model are:

- 100 1. Molecular viscosity and heat conduction is neglected since turbulent energy and momentum exchange
101 are dominant.
- 102 2. Erupted material consisting of solid with different size and mixture of gases is assumed to be well
103 mixed and behave like a single phase fluid (phase 2) which is valid for eruptions with fine particles and
104 ash.
- 105 3. Air, which is assumed to be well mixed mixture of different gases, is assumed to be another phase
106 (phase 1).
- 107 4. Assume thermodynamic equilibrium and dynamic equilibrium between the two phases. As a result,
108 both phases share the common energy equation and momentum equations.

- 109 5. All other microphysical processes (such as the phase changes of H₂O aggregation, disaggregation,
 110 absorption of gas on the surface of solids, solution of gas into a liquid) and chemical processes are not
 111 considered in this model.
 112 6. The effect of wind, is also not yet considered in this model.

Based on above assumptions, the governing equations of our model are given as:

$$\frac{\partial \rho}{\partial t} + \nabla \cdot (\rho \mathbf{v}) = 0 \quad (1)$$

$$\frac{\partial \rho \xi}{\partial t} + \nabla \cdot (\rho \xi \mathbf{v}) = 0 \quad (2)$$

$$\frac{\partial \rho \mathbf{v}}{\partial t} + \nabla \cdot (\rho \mathbf{v} \mathbf{v} + p \mathbf{I}) = \rho \mathbf{g} \quad (3)$$

$$\frac{\partial \rho E}{\partial t} + \nabla \cdot [(\rho E + p) \mathbf{v}] = \rho \mathbf{g} \cdot \mathbf{v} \quad (4)$$

- 113 where ρ is the density, \mathbf{v} is the velocity, ξ is the mass fraction of ejected material, \mathbf{g} is the gravitational
 114 acceleration, \mathbf{I} is a unit tensor. $E = e + K$ is the total energy which is a summation of kinetic energy K
 115 and internal energy e . An additional equation is required to close the system. In this model, the equation
 116 for closing the system is the following EOS (equation of state).

$$p = (\gamma_m - 1) \rho e \quad (5)$$

- 117 where

$$\gamma_m = R_m / C_{vm} + 1 \quad (6)$$

$$R_m = \xi_g R_g + \xi_a R_a \quad (7)$$

$$C_{vm} = \xi_s C_{vs} + \xi_g C_{vg} + \xi_a C_{va} \quad (8)$$

$$\xi_a = 1 - \xi \quad (9)$$

$$\xi_g = \xi \cdot \xi_{g0} \quad (10)$$

$$\xi_s = \xi - \xi_g \quad (11)$$

- 123 where, C_v is the specific heat with constant volume, R is the gas constant. ξ is the mass fraction of erupted
 124 material. The subscript m represents mixture of ejected material and air, s represents solid portion in the
 125 ejected material, g represents gas portion in the ejected material, a represents air, 0 represents physical
 126 properties of erupted material. ξ_{g0} is the mass fraction of vapor in the erupted material.

- 127 Three different boundary conditions are applied in this model. At the vent, temperature of erupted
 128 material T , eruption velocity \mathbf{v} , the mass fraction of vapor in erupted material ξ_{g0} and mass discharge
 129 rate \dot{M} are given. The pressure of erupted material p is assumed to be the same as ambient pressure for
 130 pressure-balanced eruption. The radius of vent is determined from ρ , \dot{M} and \mathbf{v} . Non-slip wall boundary
 131 condition is applied to the flat ground, where we enforce the velocity to be zero. With further assumption
 132 that the ground is adiabatic, internal energy flux, which consists of heat flux and energy flux carried by
 133 mass flux, vanishes on the wall boundary. Pressure outlet boundary condition is applied to the surrounding
 134 atmosphere where the pressure is given. Except for the pressure, boundary values for density, velocity, and

135 energy are determined by numerical calculation naturally. The initial condition for Plume-SPH is created
 136 based on atmosphere profile before the eruption.

137 The governing equations, EOS, boundary conditions, and initial conditions establish a complete mathe-
 138 matic model. The model is then discretized using smoothed particle hydrodynamics (SPH) method. The
 139 computational domain is discretized by SPH particles. The current version, Plume-SPH 1.0 (Cao et al.,
 140 2018), uses two types of SPH particles: 1) particles of phase 1 to represent ambient air, and 2) particles of
 141 phase 2 to represent erupted material. So before the eruption, the computational domain is fully occupied
 142 by particles of phase 1. During the eruption, particles of phase 2 are injected into the computational domain.
 143 The discretized model is then converted into computational software (Plume-SPH) based on a parallel data
 144 management framework (Cao et al., 2017).

145 The input parameters for Plume-SPH include the eruption condition at vent, the material properties, and
 146 atmosphere profile. The eruption parameters, material properties and atmosphere for the “Strong plume–no
 147 wind” case in the recent comparison study on eruptive column models (Costa et al., 2016) are adopted.
 148 Eruption conditions and material properties are listed in Table 3. Note that the density of erupted material
 149 at the vent and radius of the vent can be computed from the given parameters. The eruption pressure is
 150 assumed to be the same as the atmospheric pressure at the vent, hence is not given in the table. The vertical
 151 profiles of atmospheric properties were based on the reanalysis data from ECMWF (European Centre for
 152 Medium-Range Weather Forecasts) for the period corresponding to the climactic phase of the Pinatubo
 153 eruption.

154 Running of Plume-SPH essentially updates physics quantities, such as temperature, velocity, and the
 155 position of SPH particles in each time step. During Plume-SPH simulation, SPH particles of phase 2, which
 156 represent the erupted material, are injected from the eruption vent into the computation domain with an
 157 initial injection velocity. As they moving upwards, these particles will get mixed with SPH particles of
 158 phase 1, which represent the air, during the whole simulation. Their physics quantities get updated as well.
 159 After the simulation, the computation domain will be filled with SPH particles of both phase 1 and phase 2.
 160 Removing all SPH particles of phase 1 from the computation domain, all of the left SPH particles are these
 161 particles that represent the erupted material, which naturally forms a plume (see Fig. 1).

162 2.2 Puff and Initial Ash Cloud

163 Puff (Tanaka, 1991; Searcy et al., 1998) is a dynamic pollutant tracer model. the model is based on a 3D
 164 Lagrangian form of the fluid mechanics, in which the material transport is represented by the fluid motion,
 165 and diffusion is parameterized by a stochastic process of random walk. Here, the model is constructed by a
 166 sufficiently large number of Lagrangian tracer particles with a random variables $\mathbf{R}_i(t) = (x(t), y(t), z(t))$,
 167 where $i = 1 \sim M$, which represent position vectors of particles from the origin of the ash source at the
 168 time t . M is total number of Lagrangian tracer particles, a sample of all the ash particles.

$$169 \quad \mathbf{R}_i(t + \Delta t) = \mathbf{R}_i(t) + \mathbf{W}(t)\Delta t + \mathbf{Z}(t)\Delta t + \mathbf{S}_i(t)\Delta t \quad (12)$$

170 Here, \mathbf{W} accounts for wind advection, \mathbf{Z} is generated by Gaussian random numbers and accounts for
 171 turbulent dispersion, and \mathbf{S} is the terminal gravitational fallout velocity or settling speed, which depends on
 172 a tracer’s size.

173 To start a Puff simulation, it requires a collection of tracer particles as the initial condition. The tracer
 174 particles has three basic properties, age, size and position. The age of each particle is the elapsed time
 175 from when they were released from the site. Ash particles in the initial ash cloud has zero ages. Ash size
 176 distribution is initialized using a Gaussian shape on a logarithmic scale. According to mean and standard

177 deviation provided by user, Puff will assign size to each particle. Puff initialize the position of each particle
 178 according to semiempirical expressions. The height of each particle is determined according to specified
 179 distribution from the surface ($1000\text{mbar} \cong 0\text{m}$) to the top of the plume height, H_{max} , which is given by
 180 user. Puff also supports reading predefined initial ash cloud from a file, contains the coordinates of all
 181 tracer particles.

182 The commonly used distribution in Puff is Poisson distribution. For the Poisson distribution, the vertical
 183 height of ash particles is given by Eq. (13):

$$H = H_{max} - 0.5H_{width} * P + H_{width}R \quad (13)$$

184 where P is an integral value drawn from a Poisson distribution of unit mean, R is a uniformly distributed
 185 random number between 0 and 1, H_{max} is the maximum plume height, H_{width} represents an approximate
 186 vertical range over which the ash will be distributed. For Poisson distribution, two parameters, H_{max} and
 187 H_{width} controls the vertical ash distribution. Another commonly used vertical ash distribution in VATD
 188 simulation is Suzuki. For the Suzuki plume shape (Suzuki et al., 1983), the ash mass vertical distribution is
 189 assumed to follow the Eq. (Eq. (14)):

$$Q(z) = Q_m * \frac{k^2(1 - z/H_{max})\exp(k(z/H_{max} - 1))}{H_{max} [1 - (1 + k)\exp(-k)]} \quad (14)$$

190 Where Q_m is the total mass of erupted material, k is shape factor, which is an adjustable constant that
 191 controls ash distribution with height. A low value of k gives a roughly uniform distribution of mass with
 192 elevation, while high values of k concentrate mass near the plume top. For Suzuki distribution, besides
 193 the plume height H_{max} , there is another user specified parameter, k , which also affect the vertical ash
 194 distribution.

195 Puff initialize the horizontal distribution of ash particles according to semiempirical expression as well.
 196 Puff uses a uniformly distributed random process to determine ash particle locations in a circle centered
 197 on the volcano site. The maximum radius (at plume top) at which a particle can be located is given as
 198 “horizontal spread”. The horizontal displacement from a vertical line above the volcano is a random value
 199 within a circle of which the radius equals the “horizontal spread” multiplied by the ratio of the particle
 200 height H to the maximum H_{max} , see Eq. 15. So the resulting shape of the particle distribution within the
 201 plume is an inverted cone in which particles are located directly over the volcano at the lowest level and
 202 extend out further horizontally with increasing plume height.

$$r(H) = r_{max} * H/H_{max} * R \quad (15)$$

203 where $r(H)$ is the radius of the horizontal circle, whithin which, all particles at the height of H locate.
 204 r_{max} is the horizontal spread. H is the height, R is an uniformly distributed random number between 0 and
 205 1.

206 In summary, particle distributions in the initial ash cloud generated by semiempirical expressions are
 207 controlled by several parameters. Given user has chosen Poisson distribution for particle distribution in the
 208 vertical direction, there are three user specified parameters that control the tracer particle distribution in
 209 the initial ash cloud: H_{max} , H_{width} , and r_{max} . User can optimize or calibrate these parameters to adjust
 210 the initial condition of Puff so that the simulated results match better with observations, such as satellite
 211 imagery or pilot reports. Besides the initial ash cloud, other input parameters for Puff are diffusivity in the

212 vertical and horizontal directions, start and end time of the eruption, and eruption duration. When creating
 213 initial conditions from output of Plume-SPH, the total number of Lagrangian tracers is the count of all SPH
 214 particles of phase 2 in the plume. The same total number of Lagrangian tracers are used when creating
 215 initial ash cloud based on semiempirical expressions. All input parameters for Puff are list in Table 4.

216 2.3 Creation of Initial Ash Cloud From Plume-SPH Output

217 The steps to create an initial ash cloud based on the raw output of Plume-SPH are shown in Fig. 1.
 218 The method proposed consists in generating the initial ash cloud directly from Plume-SPH, foregoing
 219 assumptions and estimates, or inverse modeling, regarding ash injection height and timing. We use Plume-
 220 SPH as an example, noting that for other 3D plume models, the steps would be similar. The initial ash
 221 cloud is created from SPH particles of phase 2, which represents the erupted material in the model.

222 After reaching the maximum rise height and starting to spread horizontally, particles of phase 2 form an
 223 initial umbrella cloud (Fig. 2). The 3D plume simulation is considered complete once the umbrella cloud
 224 begins to form. Parcels that will be transported by the ambient wind are those above the “corner” region,
 225 where mean plume motion is horizontal rather than vertical.

226 Considering that SPH particles are only discretization points, each is assigned a grain size according to a
 227 given total grain size distribution (TGSD) (Paladio-Melosantos et al., 1996), and a concentration according
 228 to the mass and volumetric eruption rate. The Plume-SPH discretization points are thus switched to Puff
 229 Lagrangian tracer particles having grain sizes and concentrations. The coordinates of these tracer particles,
 230 which are initially in the local Cartesian coordinate system of Plume-SPH, are converted into Puff’s global
 231 coordinate system, which is given in terms of (*longitude, latitude, height*). Puff takes the initial ash
 232 cloud, consisting of the collection of Lagrangian tracer particles with grain size and concentration, and
 233 propagates from time t to time $t + \Delta t$ via solution to an advection/diffusion equation.

234 To summarize, there are four steps to create an initial ash cloud from the raw output of Plume-SPH:

- 235 1. filter by SPH particle type to select SPH particles that represent erupted material (phase 2)
- 236 2. filter by a mean velocity threshold to select the upper part (above the “corner” region) dominated by
horizontal transport
- 238 3. switch SPH discretization points to Lagrangian tracer particles, by assigning grain size to each particle
- 239 4. convert coordinates of the SPH Lagrangian tracers into the VATDs’ geographic coordinate system

240 The features of the volcanic plume and resulting initial ash cloud used in the case study are shown in Fig. 2.
 241 It is important to point out that since both Plume-SPH and Puff are based on the Lagrangian method, there
 242 is no extra step of conversion between an Eulerian grid and Lagrangian particles.

243 2.4 Puff Restart

244 The plume and ash transport models are run at different time scales and length scales. The spatial and
 245 temporal resolutions of the plume simulations are much finer than those of the ash transport model. It takes
 246 tens of minutes (600s in this case) for the Pinatubo plume to reach a steady height. However the eruption
 247 persisted for a few hours (9 hours for the climactic phase of Pinatubo eruption), and it may be necessary
 248 to track ash transport for days following an eruption. At present, it is too expensive computationally to
 249 do 3D plume simulations of several hours in real time. In order to handle the difference in time scale, we
 250 mimic a continuing eruption with intermittent pulses releasing ash particles. In particular, we restart Puff at
 251 an interval of 600s, i.e., the physical time of the plume simulation to reach a steady height. At every Puff
 252 restart, we integrate the output of the last Puff simulation and Plume-SPH into a new ash cloud. This new
 253 ash cloud serves as a new initial condition with which to restart a Puff simulation. A sketch demonstrating

254 the overall restart process is shown in Fig. (3). The total number of Lagrangian tracer particles used in Puff
255 thus equals the summed number of particles in all releases. The total number of tracer particles is therefore
256 no longer a user-selected parameter. Fero et al. (2008) proposed using more realistic time-dependent plume
257 heights. We do not adopt that strategy here for simplicity, although the idea would be straightforward in
258 execution, given time-dependent eruption conditions.

3 RESULTS

259 Transport of volcanic ash resulting from the Pinatubo eruption on June 15, 1991, is simulated using two
260 different initial conditions. The first type of initial condition is created in a traditional way according to
261 key global descriptors (H_{max} , H_{width} and r_{max}) and the semiempirical plume shape expressions. We use
262 the observed top height (40km) and two other parameters assigned semiempirically (Bursik et al., 2012).
263 The second type of initial condition is created by the new method proposed in this paper. To create initial
264 conditions using the new method described in this paper, the plume rise is simulated first by Plume-SPH.
265 Then the initial ash cloud is obtained by processing the raw output of Plume-SPH following steps described
266 in Sec. 2.3. Except for initial conditions, the simulation parameters that control the VATD simulation are
267 the same for both simulations. Simulated ash transport results are compared against observations.

268 The simulation results using different initial conditions are compared with TOMS images and AVHRR
269 BTD ash cloud map imagery (Fig. 6). The differences between simulated ash transport by the “Semiempiri-
270 cal initial cloud + Puff” and “Plume-SPH+ Puff” conditions are significant. The simulated ash concentration
271 based on the initial conditions created from Plume-SPH is qualitatively closer to observation than that
272 based on the semiempirical plume shape expression. At 23 hours and 31 hours after the beginning of the
273 climactic phase, the “Plume-SPH + Puff” simulation generates ash footprints that are closer to observations,
274 especially in forecasting the location where there is a high concentration of ash. However, ash just west of
275 Pinatubo observed in satellite images does not show up in “Plume-SPH + Puff” simulation results. This
276 disparity is likely due to the fact that Pinatubo continued erupting after the climactic phase, while we only
277 simulate the climactic phase. The “Semiempirical initial cloud + Puff” simulation, however, forecasts an
278 ash distribution more spatially restricted than observation. The location of the high concentration region
279 is far northwest of observation. Around 55 hours after the beginning of the climactic phase, the disparity
280 between observation and simulation becomes more obvious. Ash in the “Semiempirical initial cloud + Puff”
281 simulation is located too far west of the observation. The high concentration area of the “Plume-SPH +
282 Puff” simulation, even though closer to observation than that of the “Semiempirical initial cloud + Puff”
283 simulation, has also propagated further than observation.

284 Except for the initial conditions, both simulations adopt the same parameters and wind field data. That is
285 to say, the only difference between these two simulations is the initial distribution of ash parcels. The main
286 difference between simulation results from the “Plume-SPH + Puff” and the “Semiempirical initial cloud +
287 Puff” runs can be directly attributed to the initial ash particle distribution, which we discuss in detail in the
288 following section.

289 3.1 Importance of Maximum Height (H_{max})

290 In this section, we discuss the vertical distribution of ash particles in the initial ash cloud. The majority of
291 volcanic ash particles are usually injected at an elevation lower than the maximum height. For instance,
292 Holasek et al. (1996a,b) reported the maximum Pinatubo plume height as $\sim 39\text{km}$ while the cloud heights
293 were estimated at $\sim 20 - 25\text{ km}$. Self et al. (1996) reported that the maximum plume height could have
294 been $> 35\text{ km}$, but that plume heights were $23 \sim 28\text{ km}$ after $\sim 15 - 16\text{ hours}$. The neutral buoyancy
295 height of the Pinatubo aerosol cloud was estimated with different methods at: $\sim 17 - 26\text{km}$ (lidar) by

296 DeFoor et al. (1992), $\sim 20 - 23$ km (balloon) by Deshler et al. (1992), $\sim 17 - 28$ km (lidar) by Jäger
297 (1992), and $\sim 17 - 25$ km (lidar) by Avdyushin et al. (1993). Based on comparison between simulated
298 clouds with early infrared satellite imagery of Pinatubo, Fero et al. (2008) reported that the majority of ash
299 was transported between 16 km and 18 km. These observations make good physical sense, as particles are
300 concentrated near the intrusion height of the umbrella cloud, not near the plume top, because the plume top
301 is due to momentum overshoot. However, the empirical expressions for the height-MER relation, which
302 are commonly adopted to create initial conditions for VATD simulations, tend to place the majority of ash
303 particles closer to the top if one uses observed maximum height in the empirical expressions.

304 Here we investigate two commonly used plume shapes, the Poisson and Suzuki. Particle distributions
305 (in terms of mass percentage or particle number percentage) in the vertical direction in the initial ash
306 cloud are shown in Fig. 7. In that figure, the vertical particle distribution based on Plume-SPH output is
307 compared with the vertical particle distribution created based on semiempirical shape expressions. Both
308 Poisson and Suzuki distributions in Fig. 7 take $H_{max} = 40$ km, which is close to the reported observation
309 of maximum height. When adopting the Poisson distribution, see (c) in Fig. 7, the majority of the particles
310 are between $30\text{km} \sim 40\text{km}$. Obviously, the Poisson function distributes the majority of ash at a higher
311 elevation than was observed (e.g. Fero et al., 2008). As for the Suzuki distribution, (d) in Fig. 7, the
312 majority of ash particles also occur in a range that is significantly higher than 25 km. As for initial ash
313 clouds based on Plume-SPH simulation, most ash particles are distributed between $\sim 17 - 28$ km, which
314 matches well with observations. The maximum height is also consistent with observation. To summarize,
315 using a semiempirical plume shape expression generates an unrealistic initial ash cloud even if we use the
316 observed maximum plume height.

317 For the Poisson and Suzuki distributions, the maximum in ash particles cannot be lower without changing
318 the maximum height. To distribute the majority of ash particles at a lower elevation, the maximum height
319 must be reduced to a value smaller than the observed maximum height. Adjusting parameters such as
320 maximum height in the empirical expression is actually the traditional source term calibration method. A
321 set of initial ash clouds using different maximum heights based on the Poisson distribution is shown in Fig.
322 8). The maximum heights adopted in plume shape expressions are not obtained from any plume model or
323 observation of plume height, but by *a posteriori* calibration to later-observed ash cloud transport heights.

324 The ash clouds created by the Poisson distribution with different maximum heights are used as initial
325 conditions in Puff simulations, whose results are shown in Fig. 11. Except for the maximum height, all
326 other parameters for creating an initial ash cloud are the same as those in Table 4. Of course, the range
327 over which the majority of ash particles is located is lower when using lower maximum heights. Figure
328 11 thus shows that the maximum height has a significant influence on the ash transport simulation. When
329 the maximum height is 10 km, the high concentration area lags behind that observed. If the designated
330 maximum height is 35 km, the high concentration area propagates faster and is more spatially confined than
331 observed. When using a maximum height of ~ 41000 m, the high concentration area propagates faster and
332 the footprint is narrower than in both observation and “Plume-SPH + Puff” simulation results (see Fig. 6).
333 The simulated high concentration area is closest to “Plume-SPH + Puff” simulation results when assigning
334 a maximum height of 30 km. The low-concentration front of the volcanic ash cloud propagates faster than
335 observed, and is located far west of the high concentration areas. A low concentration tail area also appears
336 in the simulation results while there is no such tail in the observed imagery, although this could be the
337 result of imagery calibration or sensitivity. Simulation results based on a calibrated maximum height of 30
338 km show a footprint similar to those of “Plume-SPH + Puff”, although smaller in terms of area. However,
339 the initial ash cloud created by a Poisson distribution with maximum height around 20 km generates the

best match ash with observation. That is to say, a maximum height lower than the real maximum height is required by the Poisson plume shape to distribute ash particles at elevations comparable to the “true” ash distribution. Our hypothesis regarding the disparity between the “Semiempirical initial cloud + Puff” simulations and observation is confirmed. Since the initial condition of vertical ash distribution has such a dominant effect on VATD simulation, it is critical for the forecast capability of VATD simulations to explore more accurate and adaptive ways for establishing the initial ash distribution, especially methods that do not rely on *a posteriori* parameter calibration or inversion.

3.2 Effect of Vertical Spread (H_{width})

In the previous section, we explored the effects of adjusting the maximum height to change the vertical ash distribution at the source. In this section, we investigate the importance of another parameter in the semiempirical Poisson expression. We vary the “vertical spread” (H_{width} in Puff) in the range $\sim 3 - 10$ km. A set of initial ash clouds with different vertical spreads are shown in Fig. 8. Except for vertical spread, all other parameters for creating an initial ash cloud are the same as those in Table 4. The vertical width of the region within which the majority of ash particles are located becomes narrower when a smaller value for the vertical spread parameter is used, but changing it has no obvious effect on the height at which the largest fraction of ash particles is injected (essentially the height of a mode in ash distribution). The ash clouds based on different vertical spread parameters are then used as initial conditions in Puff simulations.

The results are shown in Fig. 11. Adjusting of the vertical spread changes particle distribution in the vertical direction, and thus, not surprisingly affects the VATD simulation results. None of the VATD simulations based on initial ash clouds with vertical spreads equal to 3, 5 or 10 km yield better results than do VATD simulations based on initial conditions created by Plume-SPH (see Fig. 11).

The calibration tests on vertical spread, carried out here, are certainly not exhaustive. One could do a more comprehensive calibration throughout the multi-dimensional parameter space (for Poisson distribution, the parameter space is two dimensional) and find better results. In addition, with a more complicated semiempirical plume shape expression, one could have more control over plume shape and might be able to get an initial condition that yields a more accurate ash transport forecast. However, more complicated and adaptable plume shape expressions imply a higher dimensional parameter space, which requires more effort in calibration, even though the degrees of freedom to adjust plume shape are still limited. Creating initial conditions based on 3D plume simulations is more adaptive to various cases and yields results as good as or better than calibration of the poorly-constrained semi-empirical parameter, vertical spread.

3.3 Horizontal Ash Distribution

The differences between the semiempirical plume particle distribution and actual (or simulated by the 3D plume model) are not only in the vertical direction. The importance of the horizontal distance of each initial ash particle from a line extending upward from the volcano is investigated in this section. Puff uses a uniformly distributed random process to determine ash particle locations in a circle centered on the volcano site as described in section 2.2. For the output of Plume-SPH, an effective (maximum) radius is determined according to a given threshold of ash concentration, following Cerminara et al. (2016b). A time averaged, spatial integration of the dynamic 3D flow field is conducted to remove significant fluctuations in time and space. Fig. 9 compares radius of the initial ash clouds created by 3D plume simulations with that assumed in the semiempirical plume shape expression adopted in Puff. It is impossible for the simple, assumed plume shapes to capture the complex and more realistic shapes developed by Plume-SPH. Additional parameterization may generate more reasonable shapes, but these would continue to be *ad hoc*, none would likely to have the potential fidelity of the 3D simulation to reality, and adding a temporally changing distribution would be difficult.

384 Comparison between cross-sectional views of the initial ash clouds is shown in Fig. 10. The cross-
385 sectional view of horizontal particle distribution using the semiempirical method (last figure in Fig. 10)
386 is similar to a cross-sectional view of a simulated 3D plume, in a general sense. However, for simulated
387 3D plumes, the ash particle distribution in cross section varies with height, which factor would become
388 increasingly important with increasing wind speed, were wind speed to be included in the estimate of initial
389 plume shape. It is difficult for the semiempirical expressions to accommodate such a complex distribution.

390 Despite the obvious difficulty of correctly estimating ash distribution near the vent, or for short propagation
391 times, assigning different values for the horizontal spread has a negligible effect on VATD simulation
392 results at large time. We investigated horizontal spread values between 50 km and 1600 km to create initial
393 ash clouds; all of them generated similar results at large propagation times (> 1 day). Figure 11 shows two
394 different simulation results based on initial ash clouds with horizontal spread equal to 50 km and 600 km,
395 respectively. No visible differences are apparent between them. This implies that horizontal distribution
396 has a less significant influence on VATD simulation results than does vertical distribution for long distance
397 or large time. Perhaps the most important ramification of this result is that it means the time at which the
398 “handshake” is made between Plume-SPH and the VATD does not affect results significantly for relatively
399 large distances and times.

4 DISCUSSION

4.1 Sensitivity Analysis of Other Parameters

401 Besides the positions of particles in the initial ash cloud, other parameters for Puff simulations are:
402 horizontal diffusivity, vertical diffusivity, mean grain size, grain size standard deviation and total number
403 of tracers. We present in this subsection informal but systematic sensitivity studies on these parameters.
404 We also investigate the influence of eruption duration. The sensitivity analyses will serve as the basis for
405 identifying possible sources of disparities between simulation and observation.

406 The sensitivity analyses illustrate that adjustment of parameters other than the positions of particles in
407 the initial ash cloud produces negligible visual differences in VATD simulation results. Using horizontal
408 diffusivities in the range of $[100, 100000] m^2 s^{-1}$ and vertical diffusivities in the range of $[1, 20] m^2 s^{-1}$
409 produces visually negligible differences. The simulated eruption duration should depend on either the total
410 observed duration or the duration of the climactic phase. We conducted several simulations with eruption
411 duration varying in the range of $[5, 11]$ hours with slightly different starting time of climactic phase. Table
412 2 lists all these simulations. However, only slight visible differences are observed among the simulated ash
413 transport outputs. The mean of the grain size distribution also has visually negligible effects on long-term
414 ash transport, according to our sensitivity tests in which we varied the log mean (base 10) grain radius in
415 the range of $[-7.3, -3.5] m$. The standard deviation, when varying in the range of $[0.1, 10] m$, generates a
416 negligible difference on long-range ash transport as well. A similar conclusion on parameter sensitivity is
417 reported by Fero et al. (e.g. 2008); Daniele et al. (e.g. 2009). Among the parameters explored, the eruption
418 duration and beginning time show the most obvious influence on simulated ash distribution, although the
419 effect is still small. To show the differences in an intuitive way, (a) - (c) in Fig. ?? shows simulated ash
420 distribution corresponding to 4.9 hours duration, 9 hours duration and 11 hours duration, respectively.
421 After 72 hours, relative to the simulation starting time, these three cases generate very similar results
422 with tiny visible differences. To summarize, all these parameters have negligible effects on long-term ash
423 distribution.

424 The new methodology for generating initial ash clouds introduces a new parameter: elevation threshold,
425 which is the lower elevation limit of the ash that will be transported by the VATD. This parameter needs to be

426 specified at this time, as there is no *a priori* way to define it, given the continuous vertical distribution of ash
427 in the eruption column. We carry out a separate, informal sensitivity analysis on this parameter by varying
428 the elevation threshold from 1500 m (the height of the vent) to 25000 m. The simulated ash distributions
429 show obvious visible differences. Such influence is especially obvious when the elevation threshold is
430 either very high or very low. However, varying the elevation threshold in the range of [12000, 18000] m
431 generates relatively small differences in ash transport simulation results. Figure 4 (d) and (e) compare the
432 simulated ash distributions corresponding to elevation thresholds of 1500 m and 15000 m. Compared with
433 the ash distribution for a threshold of 25000 m, an extra long tail appears when using an elevation threshold
434 of 1500 m. Adopting lower elevation thresholds adds more tracer particles at lower elevation. As the winds
435 at different elevations are different, the tracers at lower elevations propagate in different directions. The
436 HYSPLIT (Stein et al., 2015; Rolph et al., 2017) forward trajectory tracking starting at 1624 UTC on
437 June 15, indicates that the wind between elevations of 10000 m and 15000 m blew from north-east to
438 south-west, while winds of higher elevation blew from east to west (see Fig. 5). The results suggest that the
439 elevation threshold is best estimated from the height at which the parcel number or mass concentration has
440 an inflection point in the vertical distribution (*cf.* Figure 4(d) and (e)). Below this inflection point, particle
441 trajectories are primarily vertical in the stalk-like eruption column. Above this level, particle trajectories
442 are primarily horizontal, as they flow into the umbrella cloud gravity current.

443 The sensitivity analyses demonstrate that the initial conditions for the VATD simulations, derived from
444 the plume model, have the most significant effect on simulated ash propagation, while all other input
445 parameters have negligible influence. An initial ash cloud generated based on the semiempirical expression,
446 which is a function of several parameters, often differs significantly from a realistic initial ash cloud. Such
447 initial conditions might greatly compromise the accuracy of a VATD simulation.

448 In this paper, we do not carry out any sensitivity investigation with respect to wind field, even though it is
449 a dominant factor in a VATD simulation. In the present case study, we use global NOAA/OAR/ESRL6–
450 h , 2.0° reanalysis wind field data (Whitaker et al., 2004; Compo et al., 2006, 2011).

451 4.2 Summary

452 This paper presents, for the first time, VATD simulations using initial source conditions created by a 3D
453 plume model. Traditional VATD simulations use initial conditions created according to a semiempirical
454 plume shape expression. A case study of the 1991 Pinatubo eruption demonstrates that a 3D plume model
455 can create more realistic initial ash cloud and ash parcel positions, and therefore improve the accuracy of
456 ash transport forecasts. Informal sensitivity analyses suggest that initial conditions, as expressed in the
457 disposition of initial ash parcel positions in the vertical, have a more significant effect on a volcanic ash
458 transport forecast than most other parameters. Comparison of initial ash parcel distributions among the
459 3D plume model, semiempirical expressions, and observations suggests that a major subpopulation of ash
460 parcels should be placed at a much lower elevation than maximum height to obtain a better VATD forecast.
461 For the Pinatubo case study, “well-matched” simulation results are observed when using a maximum height
462 of around 30km in semiempirical expressions, which is much lower than the observed maximum height of
463 40km. Comparing the effects of the maximum height, vertical spread and horizontal spread shows that ash
464 particle distribution in the vertical direction has the strongest effect on VATD simulation.

465 To summarize, we have presented a novel method for creating *a priori* initial source conditions for
466 VATD simulations. We have shown that it might be possible to obtain initial positions of ash parcels
467 with deterministic forward modeling of the volcanic plume, potentially obviating or lessening the need to
468 attempt to somehow observe initial positions, or *a posteriori* create a history of release heights via inversion
469 (Stohl et al., 2011). Although the method now suffers from the high computational cost associated with

470 3D forward modeling, there is the possibility that in future it might not only help overcome shortcomings
471 of existing methods used to generate *a priori* input parameters, but also overcome the need to do the
472 thousands of runs associated with inverse modeling. In addition, computational cost will continue to
473 diminish as computing speed increases. As they are forward numerical models based on first principles,
474 3D plume models need little if any parameterization, and user intervention should not be required to
475 improve forecast power; no assumption about the initial position of ash parcels is needed. Generation of the
476 initial cloud of ash parcels directly by 3D simulation is potentially adaptable to a variety of volcanic and
477 atmospheric scenarios. In contrast, semiempirical expressions used to determine initial conditions require
478 several parameters to control ash particle distribution along a vertical line source or some simplified shape
479 of the initial ash cloud, making it difficult in some cases to generate initial conditions that closely resemble
480 a complex reality.

481 The full range of research issues raised by numerical forecasting of volcanic clouds is diverse. We
482 described in this paper the effect of initial conditions chosen from the output of a 3D plume model on
483 numerical forecasts of volcanic ash transport simulations. The wind field, another important factor in
484 volcanic ash transport simulations, is not discussed in the present work. Some other aspects, such as
485 microphysical processes, even though they play lesser roles, likely need to be included in VATDs to
486 improve accuracy for a particular eruption. In addition, eruption conditions are subject to change with time,
487 even during the climactic phase of an eruption. In the future, time-dependent initial conditions for VATDs
488 can be created from 3D plume simulations with time-dependent eruption conditions.

CONFLICT OF INTEREST STATEMENT

489 The authors declare that the research was conducted in the absence of any commercial or financial
490 relationships that could be construed as a potential conflict of interest.

AUTHOR CONTRIBUTIONS

491 The idea of using 3D plume model to start a VATD simulation originated from a conservation between AP
492 and MB. ZC carried out the Plume-SPH simulations, PUFF simulations, results analysis, and prepared the
493 first draft. All authors worked together for further revisions. MB carried out the HYSPLIT simulation. QY
494 post processed the PUFF simulation results, overlapped the simulation results with satellite observation.
495 All authors contributed equally to the manuscript writing. AP and MB obtained funding to financially
496 support the work.

FUNDING

497 This work was supported by National Science Foundation awards 1521855, 1621853, and 1821311,
498 1821338 and 2004302 and by the National Research Foundation Singapore and the Singapore Ministry
499 of Education under the Research Centres of Excellence initiative (project number: NRF2018NRF-
500 NSFC003ES-010).

ACKNOWLEDGMENTS

501 Support for the Twentieth Century Reanalysis Project dataset is provided by the U.S. Department of Energy,
502 Office of Science Innovative and Novel Computational Impact on Theory and Experiment (DOE INCITE)
503 program, and Office of Biological and Environmental Research (BER), and by the National Oceanic and
504 Atmospheric Administration Climate Program Office. We are grateful to the two anonymous reviewers of
505 the paper for their constructive comments and suggestions that improved the paper.

REFERENCES

- 506 Avdyushin, S., Tulinov, G., Ivanov, M., Kuzmenko, B., Mezhuev, I., Nardi, B., et al. (1993). 1. spatial and
507 temporal evolution of the optical thickness of the pinatubo aerosol cloud in the northern hemisphere
508 from a network of ship-borne and stationary lidars. *Geophysical research letters* 20, 1963–1966
- 509 Bonadonna, C. and Houghton, B. (2005). Total grain-size distribution and volume of tephra-fall deposits.
510 *Bulletin of Volcanology* 67, 441–456
- 511 Bursik, M. (2001). Effect of wind on the rise height of volcanic plumes. *Geophys. Res. Lett* 28, 3621–3624
- 512 Bursik, M., Jones, M., Carn, S., Dean, K., Patra, A., Pavolonis, M., et al. (2012). Estimation and
513 propagation of volcanic source parameter uncertainty in an ash transport and dispersal model: application
514 to the eyjafjallajokull plume of 14–16 april 2010. *Bulletin of volcanology* 74, 2321–2338
- 515 Bursik, M., Kobs, S., Burns, A., Braitseva, O., Bazanova, L., Melekestsev, I., et al. (2009). Volcanic
516 plumes and wind: Jetstream interaction examples and implications for air traffic. *Journal of Volcanology*
517 and *Geothermal Research* 186, 60–67
- 518 Cao, Z., Patra, A., Bursik, M., Pitman, E. B., and Jones, M. (2018). Plume-sph 1.0: a three-dimensional,
519 dusty-gas volcanic plume model based on smoothed particle hydrodynamics. *Geoscientific Model
520 Development* 11, 2691–2715
- 521 Cao, Z., Patra, A., and Jones, M. (2017). Data management and volcano plume simulation with parallel
522 sph method and dynamic halo domains. *Procedia Computer Science* 108, 786–795
- 523 Cerminara, M., Esposti Ongaro, T., and Berselli, L. (2016a). Ashee-1.0: a compressible, equilibrium-
524 eulerian model for volcanic ash plumes. *Geoscientific Model Development* 9, 697–730
- 525 Cerminara, M., Esposti Ongaro, T., and Neri, A. (2016b). Large eddy simulation of gas–particle kinematic
526 decoupling and turbulent entrainment in volcanic plumes. *Journal of Volcanology and Geothermal
527 Research*
- 528 Compo, G. P., Whitaker, J. S., and Sardeshmukh, P. D. (2006). Feasibility of a 100-year reanalysis using
529 only surface pressure data. *Bulletin of the American Meteorological Society* 87, 175–190
- 530 Compo, G. P., Whitaker, J. S., Sardeshmukh, P. D., Matsui, N., Allan, R. J., Yin, X., et al. (2011). The
531 twentieth century reanalysis project. *Quarterly Journal of the Royal Meteorological Society* 137, 1–28
- 532 Costa, A., Suzuki, Y., Cerminara, M., Devenish, B., Esposti Ongaro, T., Herzog, M., et al. (2016). Results
533 of the eruptive column model inter-comparison study. *Journal of Volcanology and Geothermal Research*
- 534 D'amours, R. (1998). Modeling the etex plume dispersion with the canadian emergency response model.
535 *Atmospheric Environment* 32, 4335–4341
- 536 Daniele, P., Lirer, L., Petrosino, P., Spinelli, N., and Peterson, R. (2009). Applications of the puff model to
537 forecasts of volcanic clouds dispersal from etna and vesuvio. *Computers & Geosciences* 35, 1035–1049
- 538 DeFoor, T. E., Robinson, E., and Ryan, S. (1992). Early lidar observations of the june 1991 pinatubo
539 eruption plume at mauna loa observatory, hawaii. *Geophysical research letters* 19, 187–190
- 540 de'Michieli Vitturi, M., Neri, A., and Barsotti, S. (2015). Plume-mom 1.0: A new integral model of
541 volcanic plumes based on the method of moments. *Geoscientific Model Development* 8, 2447–2463
- 542 Deshler, T., Hofmann, D., Johnson, B., and Rozier, W. (1992). Balloonborne measurements of the pinatubo
543 aerosol size distribution and volatility at laramie, wyoming during the summer of 1991. *Geophysical
544 research letters* 19, 199–202
- 545 Draxler, R. R. and Hess, G. (1998). An overview of the hysplit_4 modelling system for trajectories.
546 *Australian meteorological magazine* 47, 295–308
- 547 Fero, J., Carey, S. N., and Merrill, J. T. (2008). Simulation of the 1980 eruption of mount st. helens using
548 the ash-tracking model puff. *Journal of Volcanology and Geothermal Research* 175, 355–366

- 549 Fero, J., Carey, S. N., and Merrill, J. T. (2009). Simulating the dispersal of tephra from the 1991
550 pinatubo eruption: implications for the formation of widespread ash layers. *Journal of Volcanology and*
551 *Geothermal Research* 186, 120–131
- 552 Folch, A., Costa, A., and Macedonio, G. (2009). Fall3d: A computational model for transport and
553 deposition of volcanic ash. *Computers & Geosciences* 35, 1334–1342
- 554 Folch, A., Costa, A., and Macedonio, G. (2016). Fplume-1.0: An integral volcanic plume model accounting
555 for ash aggregation. *Geoscientific Model Development* 9, 431
- 556 Guo, S., Bluth, G. J., Rose, W. I., Watson, I. M., and Prata, A. (2004a). Re-evaluation of so₂ release
557 of the 15 june 1991 pinatubo eruption using ultraviolet and infrared satellite sensors. *Geochemistry,*
558 *Geophysics, Geosystems* 5
- 559 Guo, S., Rose, W. I., Bluth, G. J., and Watson, I. M. (2004b). Particles in the great pinatubo volcanic cloud
560 of june 1991: The role of ice. *Geochemistry, Geophysics, Geosystems* 5
- 561 Holasek, R., Self, S., and Woods, A. (1996a). Satellite observations and interpretation of the 1991 mount
562 pinatubo eruption plumes. *Journal of Geophysical Research: Solid Earth* 101, 27635–27655
- 563 Holasek, R. E., Woods, A. W., and Self, S. (1996b). Experiments on gas-ash separation processes in
564 volcanic umbrella plumes. *Journal of volcanology and geothermal research* 70, 169–181
- 565 Jäger, H. (1992). The pinatubo eruption cloud observed by lidar at garmisch-partenkirchen. *Geophysical*
566 *research letters* 19, 191–194
- 567 Mastin, L. G. (2007). A user-friendly one-dimensional model for wet volcanic plumes. *Geochemistry,*
568 *Geophysics, Geosystems* 8
- 569 Neri, A., Esposti Ongaro, T., Macedonio, G., and Gidaspow, D. (2003). Multiparticle simulation of
570 collapsing volcanic columns and pyroclastic flow. *Journal of Geophysical Research: Solid Earth*
571 (1978–2012) 108
- 572 Oberhuber, J. M., Herzog, M., Graf, H.-F., and Schwanke, K. (1998). Volcanic plume simulation on large
573 scales. *Journal of Volcanology and Geothermal Research* 87, 29–53
- 574 Paladio-Melosantos, M. L. O., Solidum, R. U., Scott, W. E., Quiambao, R. B., Umbal, J. V., Rodolfo, K. S.,
575 et al. (1996). Tephra falls of the 1991 eruptions of mount pinatubo. *Fire and mud* 12000, 12030
- 576 Pouget, S., Bursik, M., Singla, P., and Singh, T. (2016). Sensitivity analysis of a one-dimensional model of
577 a volcanic plume with particle fallout and collapse behavior. *Journal of Volcanology and Geothermal*
578 *Research*
- 579 Rolph, G., Stein, A., and Stunder, B. (2017). Real-time environmental applications and display system:
580 Ready. *Environmental Modelling & Software* 95, 210–228
- 581 Schwaiger, H. F., Denlinger, R. P., and Mastin, L. G. (2012). Ash3d: A finite-volume, conservative
582 numerical model for ash transport and tephra deposition. *Journal of Geophysical Research: Solid Earth*
583 117
- 584 Scott, W. E., Hoblitt, R. P., Torres, R. C., Self, S., Martinez, M. M. L., and Nillos, T. (1996). Pyroclastic
585 flows of the june 15, 1991, climactic eruption of mount pinatubo. *Fire and Mud: eruptions and lahars of*
586 *Mount Pinatubo, Philippines*, 545–570
- 587 Searcy, C., Dean, K., and Stringer, W. (1998). Puff: A volcanic ash tracking and prediction model. *Journal*
588 *of Volcanology and Geothermal Research* 80, 1–16
- 589 Self, S., Zhao, J.-X., Holasek, R. E., Torres, R. C., and King, A. J. (1996). The atmospheric impact of the
590 1991 mount pinatubo eruption
- 591 Stein, A., Draxler, R., Rolph, G., Stunder, B., Cohen, M., and Ngan, F. (2015). Noaa's hysplit atmospheric
592 transport and dispersion modeling system. *Bulletin of the American Meteorological Society* 96, 2059–
593 2077

Table 1. Three different methods for creating initial conditions (initial ash clouds) for Puff simulation

	No model	1D model	3D model
Maximum height	Calibration	Semiempirical	1st principle
Average height	Calibration	Conservation (1D)	laws 1st principle
Vertical spread	Calibration	Semiempirical	1st principle
Column radius	Calibration	Conservation (1D)	laws 1st principle
Plume shape	Semiempirical	Semiempirical	1st principle
Tracers number	Free parameter	Free Parameter	Based on simulation

- 594 Stohl, A., Prata, A., Eckhardt, S., Clarisse, L., Durant, A., Henne, S., et al. (2011). Determination of
 595 time-and height-resolved volcanic ash emissions and their use for quantitative ash dispersion modeling:
 596 the 2010 eyjafjallajökull eruption. *Atmospheric Chemistry and Physics* 11, 4333–4351
- 597 Suzuki, T. et al. (1983). A theoretical model for dispersion of tephra. *Arc volcanism: physics and tectonics*
 598 95, 113
- 599 Suzuki, Y. and Koyaguchi, T. (2009). A three-dimensional numerical simulation of spreading umbrella
 600 clouds. *Journal of Geophysical Research: Solid Earth (1978–2012)* 114
- 601 Suzuki, Y. J., Koyaguchi, T., Ogawa, M., and Hachisu, I. (2005). A numerical study of turbulent mixing
 602 in eruption clouds using a three-dimensional fluid dynamics model. *Journal of Geophysical Research: Solid Earth* 110
- 603
- 604 Tanaka, H. (1991). Development of a prediction scheme for the volcanic ash fall from redoubt volcano. In
 605 *First Int'l. Symp. on Volcanic Ash and Aviation Safety*. vol. 58
- 606 Tupper, A., Itikarai, I., Richards, M., Prata, F., Carn, S., and Rosenfeld, D. (2007). Facing the challenges of
 607 the international airways volcano watch: the 2004/05 eruptions of manam, papua new guinea. *Weather and Forecasting* 22, 175–191
- 608
- 609 Walko, R., Tremback, C., and Bell, M. (1995). Hypact: The hybrid particle and concentration transport
 610 model. *User's guide*
- 611 Whitaker, J. S., Compo, G. P., Wei, X., and Hamill, T. M. (2004). Reanalysis without radiosondes using
 612 ensemble data assimilation. *Monthly Weather Review* 132, 1190–1200
- 613 Witham, C., Hort, M., Potts, R., Servranckx, R., Husson, P., and Bonnardot, F. (2007). Comparison of
 614 vaac atmospheric dispersion models using the 1 november 2004 grimsvötn eruption. *Meteorological Applications* 14, 27–38
- 615
- 616 Woods, A. (1988). The fluid dynamics and thermodynamics of eruption columns. *Bulletin of Volcanology*
 617 50, 169–193
- 618 Zidikheri, M. J., Lucas, C., and Potts, R. J. (2017). Estimation of optimal dispersion model source
 619 parameters using satellite detections of volcanic ash. *Journal of Geophysical Research: Atmospheres*
 620 122, 8207–8232

FIGURE CAPTIONS

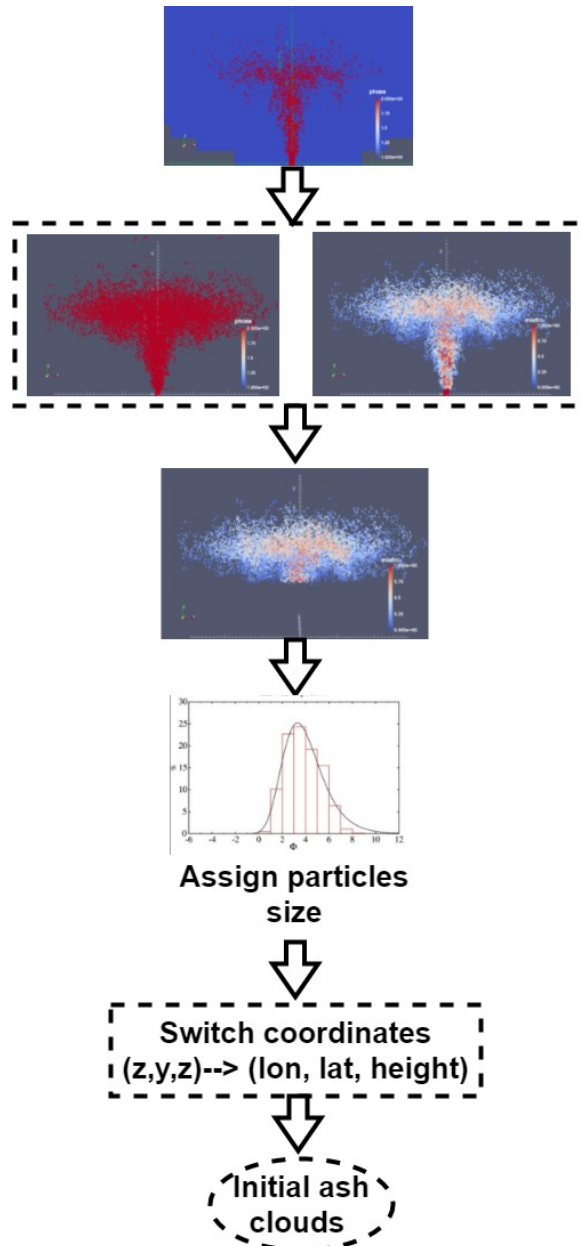


Figure 1. Steps to create initial condition for Puff based on raw output of Plume-SPH (Cao et al., 2018). First row: raw output of Plume-SPH. Blue particles are phase 1 (ambient air), red particles are phase 2 (erupted material). Second row: plume after removing SPH particles of phase 1. Picture at right is colored according to the mass fraction of erupted material. Third row: volcanic plume above the “corner” region after cutting off the lower portion. Fourth row: assign sizes to particles converting numerical discretization points into tracers. Fifth row: switch coordinates in local coordinate system into (*longitude, latitude, height*)

Table 2. The starting and ending time (UT) for simulating the climactic phase of Pinatubo eruption on June 15 1991. Observed plume height (Holasek et al., 1996a) at different time are also listed in the table.

Eruption duration	4.9 hours	9 hours	10 hours	11.1 hours
Start time	0441	0441	0441	0334
Height at start time	37.5 km	37.5 km	37.5 km	24.5 km
End time	0934	1341	1441	1441
Height at end time	35 km	26.5 km	22.5	22.5 km

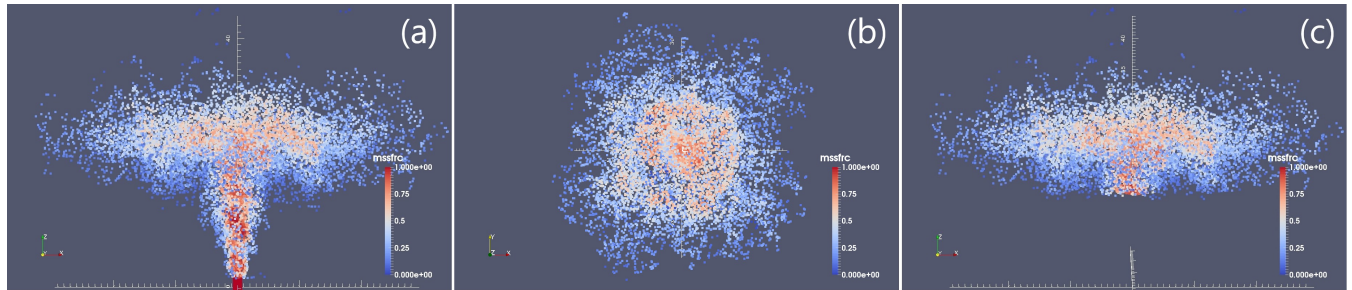


Figure 2. Volcano plume from 3D plume model. All particles in the pictures are of phase 2 (particle of phase 1 has been removed) at 600s after eruption, at which time, the plume has already reached the maximum height and started spreading radially. (a) is front view of the whole plume. (b) top view of the plume. (c) is front view of the initial ash cloud, which is essentially a portion of the whole plume with elevation higher than a given threshold (in this picture is 15000m). Particles are colored according to mass fraction of erupted material. Red represents high mass fraction while blue represents low mass fraction.

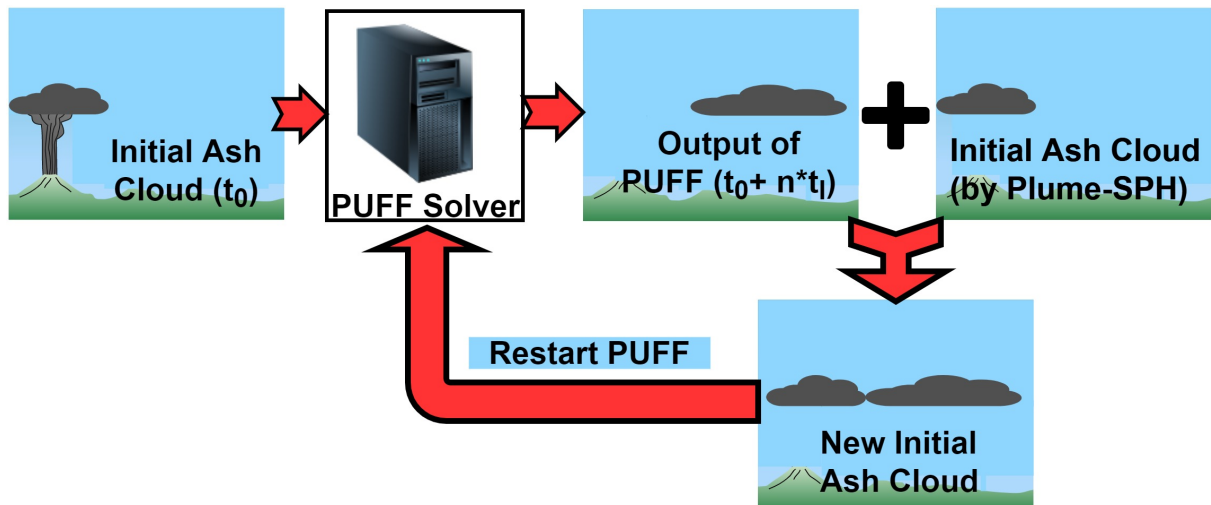


Figure 3. Mimic successive eruption with intermittent pulsed releasing of ash particles. t_l is the period of pulsing release. t_l equals the physical time of 3D plume simulation.

Table 3. List of eruption condition and material properties for plume simulation

Parameters	Units	Plume
Vent velocity	$m \cdot s^{-1}$	275
Vent gas mass fraction		0.05
Vent Temperature	K	1053
Vent height	m	1500
Mass discharge rate	$kg \cdot s^{-1}$	1.5×10^9
Specific heat of gas at constant volume	$J \cdot kg^{-1} \cdot K^{-1}$	717
Specific heat of air at constant volume	$J \cdot kg^{-1} \cdot K^{-1}$	1340
Specific heat of solid	$J \cdot kg^{-1} \cdot K^{-1}$	1100
Specific heat of gas at constant pressure	$J \cdot kg^{-1} \cdot K^{-1}$	1000
Specific heat of air at constant pressure	$J \cdot kg^{-1} \cdot K^{-1}$	1810
Density of air at vent height	$kg \cdot m^{-3}$	1.104
Pressure at vent height	Pa	84363.4

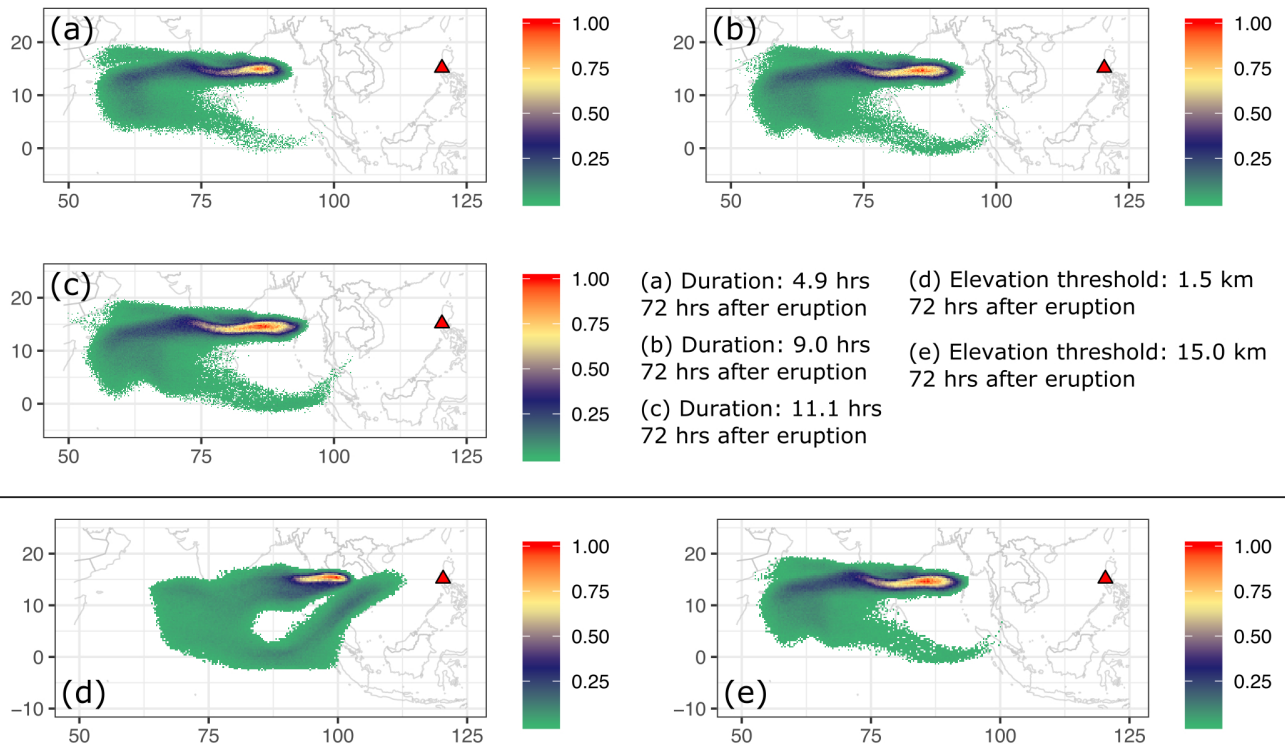


Figure 4. Sensitivity of Puff simulation with respect to eruption durations and initial ash cloud cutoff heights .(a) to (c) are simulated ash distribution with different starting and ending time. They corresponding to eruption duration of 4.9 hours, 9 hours and 11.1 hours respectively. Starting and ending time for each case is in Table 2. (d) and (e) are simulated ash distribution taking initial ash clouds obtained using different elevation thresholds (1500m and 15000 m) from output of Plume-SPH. The starting and ending time are corresponding to 9 hours duration case in Table 2. The contours correspond to ash concentration at 72 hours after eruption.

Table 4. Parameters used in VATD simulation of the climactic phase of Pinatubo eruption on June 15 1991. The first six parameters are used by semiempirical expression to create an initial ash cloud. When creating an initial condition based on the Plume-SPH model, these parameters are extracted from output of Plume-SPH model.

Parameters	Unit	Semiempirical	Plume-SPH
Maximum Height (H_{max})	m	40000	-
Horizontal Spread (r_{max})	km	103.808	-
Vertical Spread (H_{width})	km	6.662	-
Plume Shape	-	Poisson	-
Total Ash Particles	-	1768500	1768500
Elevation Threshold	m	-	15000
Horizontal Diffusivity	m^2/s	10000	10000
Vertical Diffusivity	m^2/s	10	10
Grain Size Distribution	-	Gaussian	Gaussian
Mean of Grain Size (Radius)	mm	3.5×10^{-2}	3.5×10^{-2}
Standard Deviation of Grain Size	-	1.0	1.0
Start Time	UT	0441	0441
End time	UT	1341	1341
Simulation Duration	hour	72	72

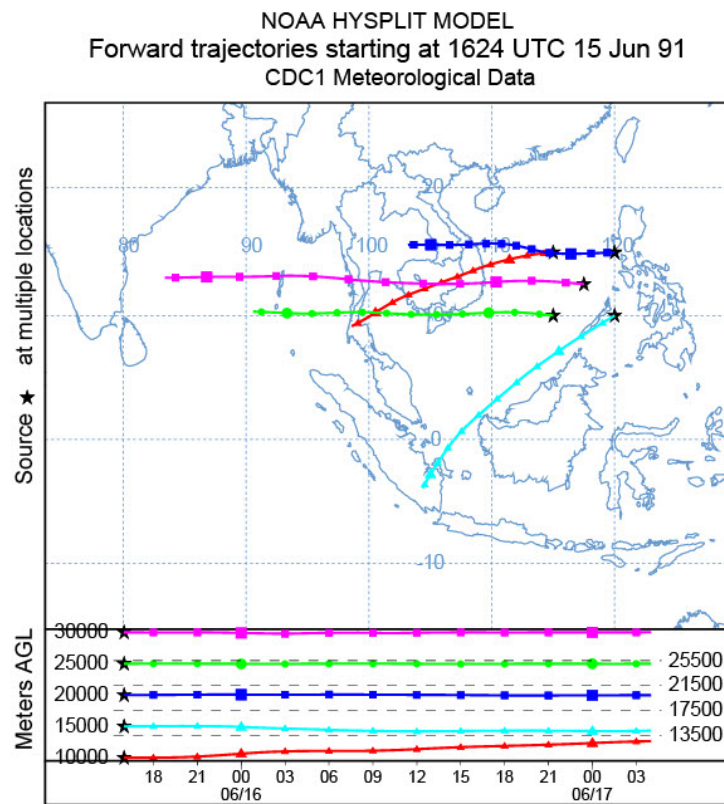


Figure 5. Trajectories of particles starting from different heights indicating the wind directions of different evaluations.

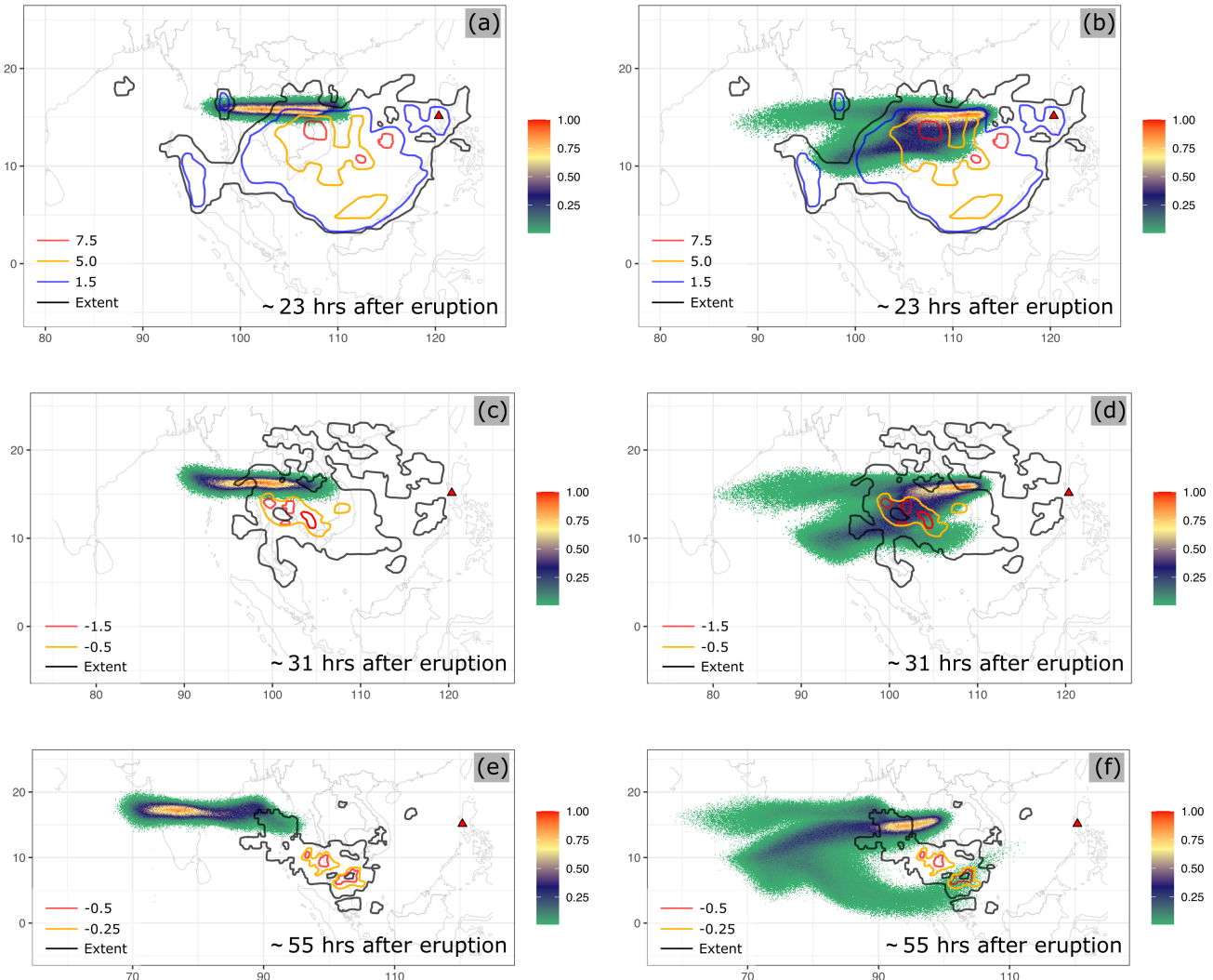


Figure 6. Comparison between “Semiempirical initial cloud + Puff” and “Plume-SPH + Puff”. Pictures to the left are: Puff simulation based on initial condition created according to semiempirical plume shape expression. Pictures to the right are Puff simulation based on initial condition generated by Plume-SPH. TOMS or AVHRR image of Pinatubo ash cloud are overlapped with the simulation results. Ash clouds at different hours after eruption are on different rows. From top to bottom, the images are corresponding to around 23 hours after eruption (UT 199106160341), 31 hours after eruption (UT 199106161141), 55 hours after eruption (UT 199106171141). The observation data on the first row are TOMS ash and ice map. The observation data on the second and third row are AVHRR BTD ash cloud map with atmospheric correction method applied (Guo et al., 2004b).

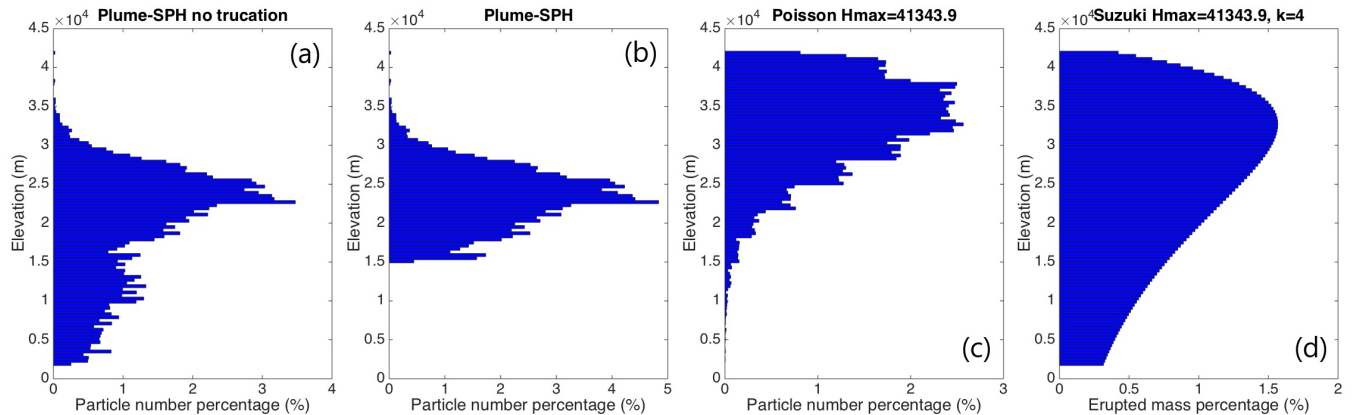


Figure 7. Particle distribution of initial ash cloud in vertical direction. (a) is corresponding to the initial ash cloud obtained from Plume-SPH output. (b) is corresponding to ash distribution of Plume-SPH output truncated by a elevation threshold of 15000m. (c) is for vertical ash distribution based on Poisson distribution with maximum height equals to 40000m. Another parameter, the vertical spread, in the expression of Poisson plume shape is 6662m. (d) is corresponding to Suzuki distribution with maximum height equals to 40000m. Another parameter in Suzuki distribution, the shape factor, is 4. The x axis is the percentage of particle numbers for Plume-SPH and Poisson. For Suzuki the x axis is the mass percentage of erupted material.

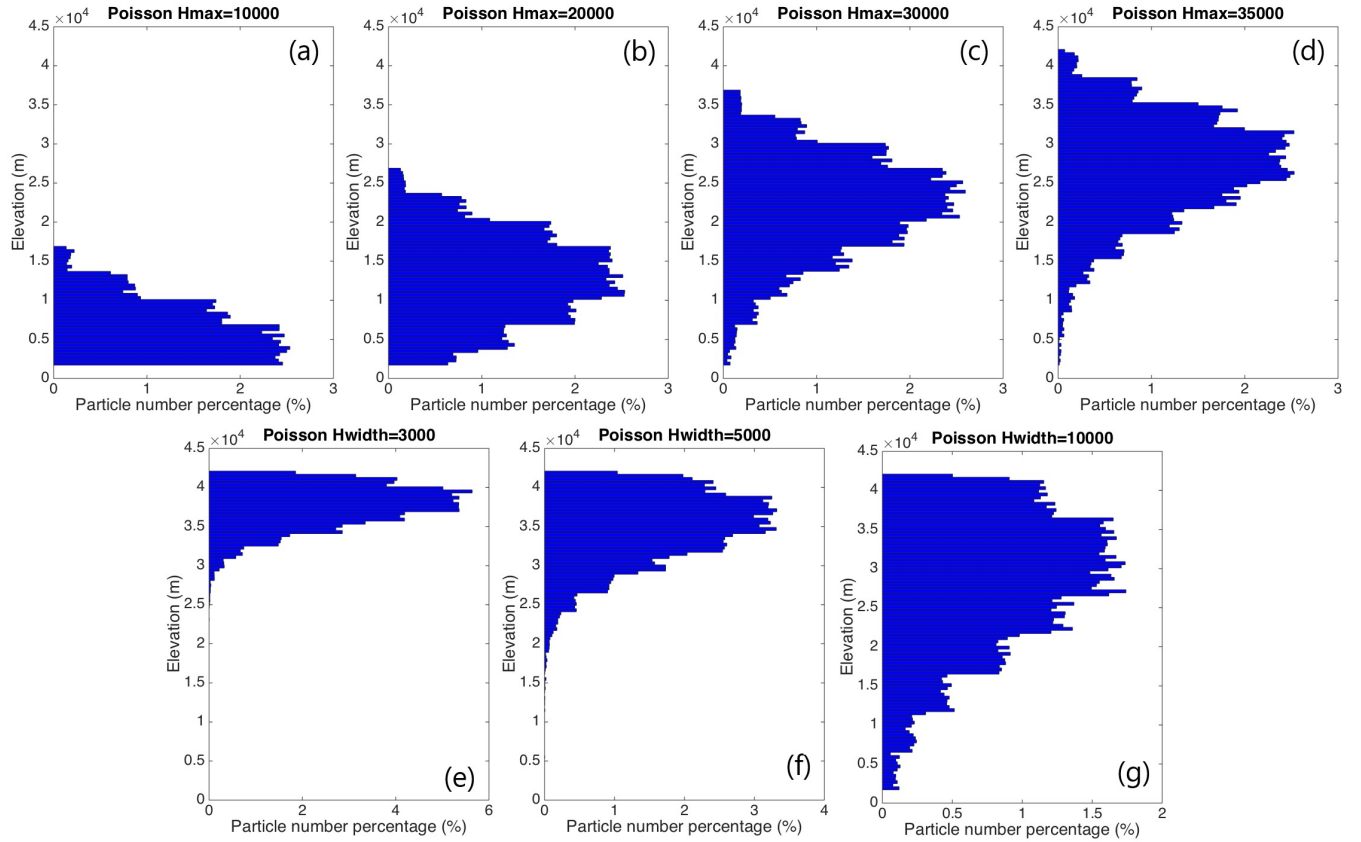


Figure 8. Initial particle distribution in vertical direction based on Poisson plume shape. The first row varies maximum heights. (a) to (d) are corresponding to maximum height of 10000m, 20000m, 30000m, 35000m. Another parameter, the vertical spread, in the expression of Poisson plume shape is 6662m for all four figures in the first row. The second row varies “vertical spread”. (e) to (g) are corresponding to vertical spread of 3km, 5km and 10km. The maximum height in the expression of Poisson plume shape is 40000m for all three figures. The x axis is the percentage of particle numbers. See Fig. 7 for vertical ash distribution of Plume-SPH output.

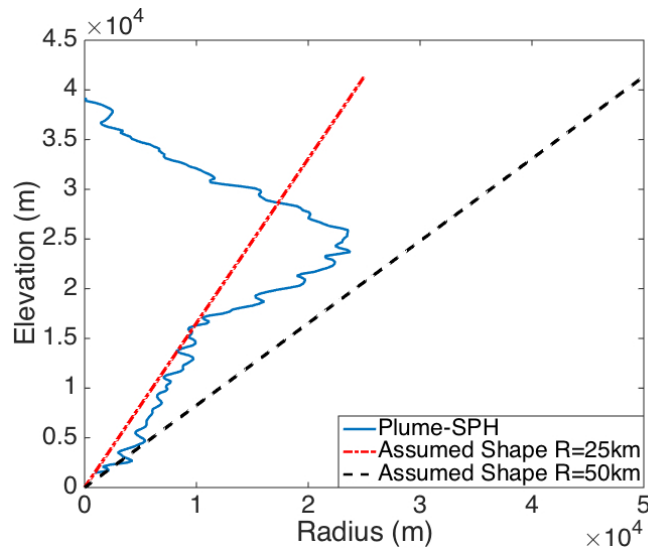


Figure 9. Comparison between radius of initial ash clouds created by 3D plume model (Plume-SPH) and assumed initial ash cloud shape in Puff. The plume shape expression used in Puff defines an inverted cone whose actual shape changes when “horizontal spread” takes different values. $R = 25\text{km}$ is corresponding to “horizontal spread” equals to 50km . $R = 50\text{km}$ is corresponding to “horizontal spread” equals to 100km

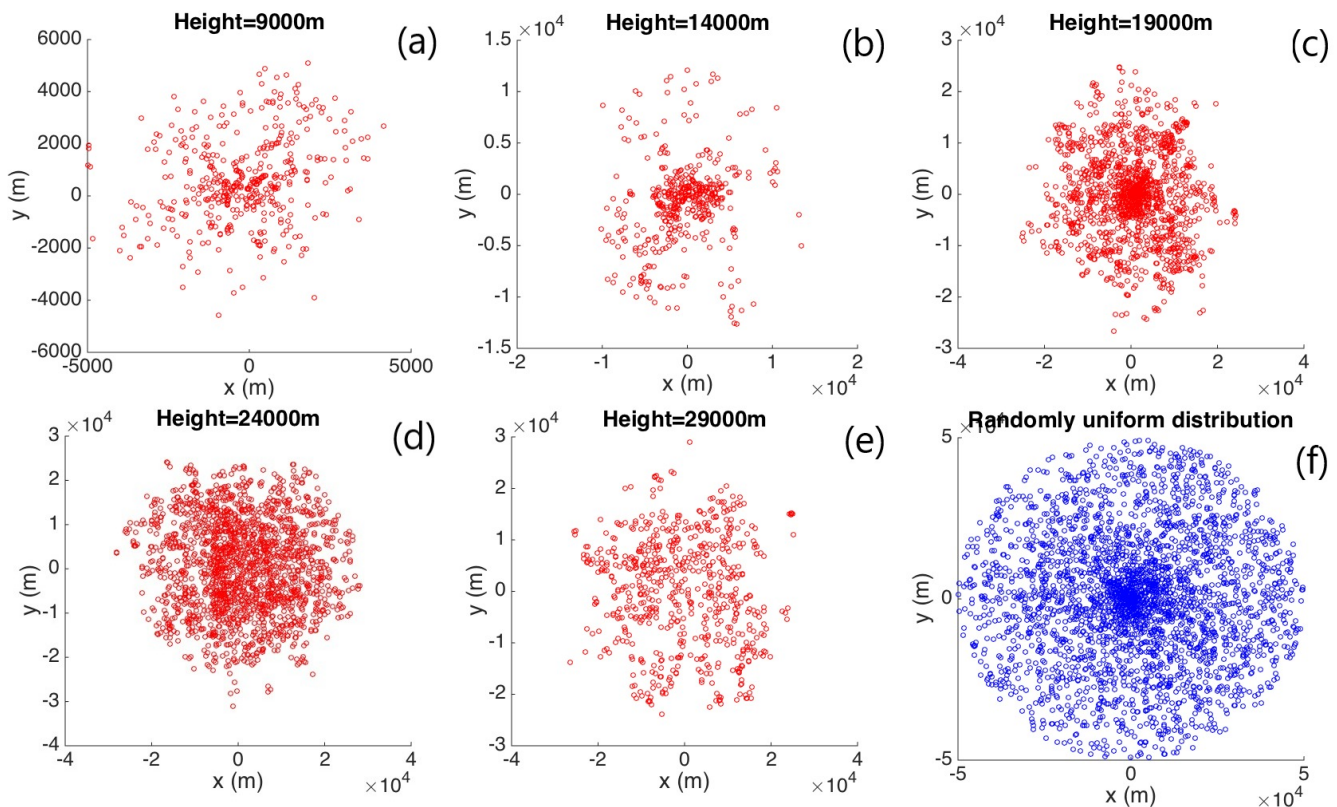


Figure 10. Horizontal distribution of ash particles (tracers) on a cross section of initial ash cloud. Puff assumes a randomly uniform distribution of ash particles within a circle, as shown by blue dots in (f). All other figures show the ash particle distribution of initial ash clouds created by Plume-SPH at different elevations.

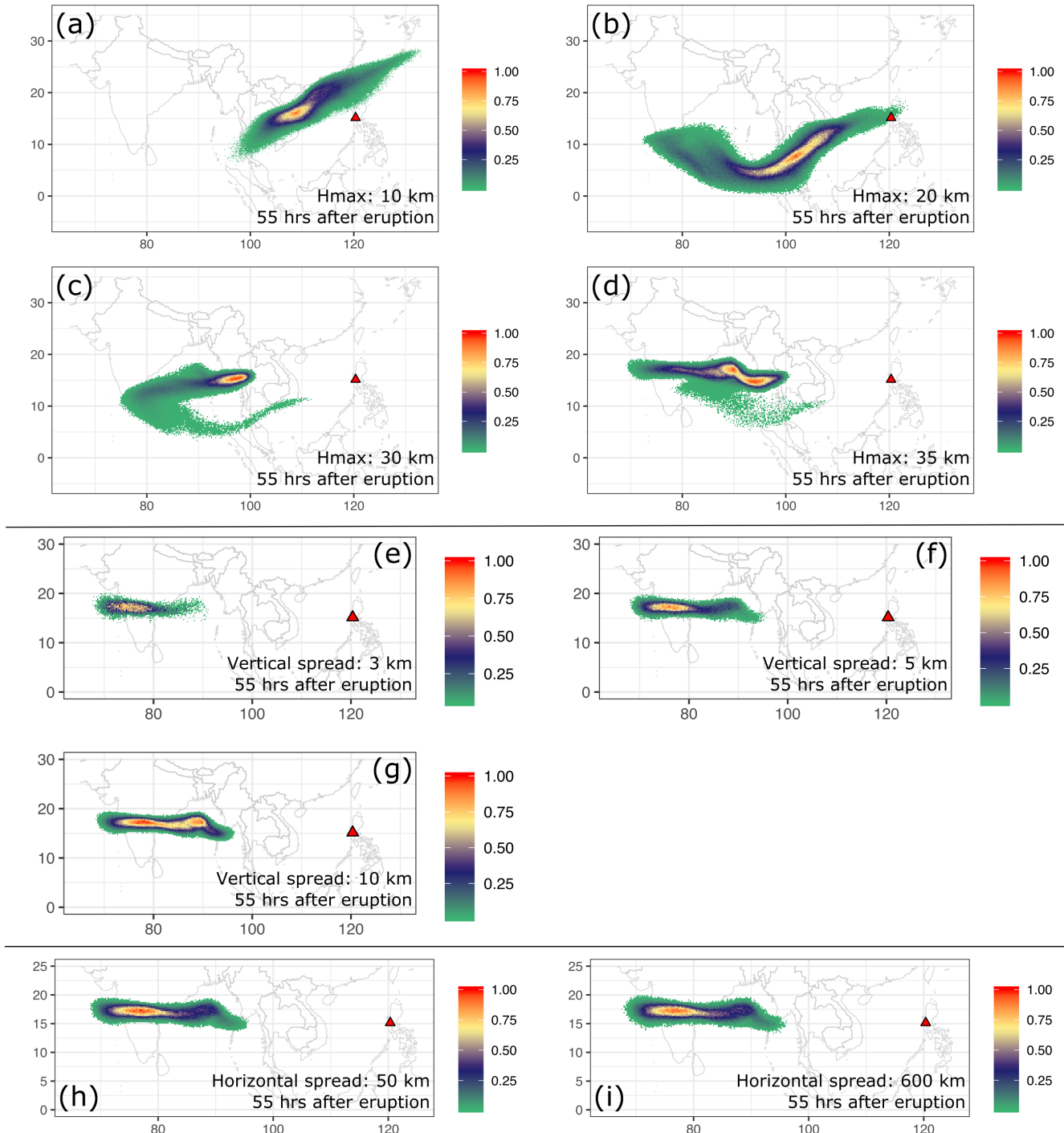


Figure 11. Ash transport simulated by Puff using different initial ash clouds created according the empirical expressions. Initial ash cloud for (a) to (d) are created according to Poisson distribution with maximum plume heights of 10km, 20km, 30km and 35km respectively. Initial ash cloud for (e) to (g) are created with vertical spread equals to 3km, 5km and 10km. respectively. Initial ash cloud for (h) - (i) are created with “horizontal spread” equals to 50km and 600km respectively. All images are for simulated ash transport around 55 hours after eruption (UT 199106171141). See the observed cloud image in Fig. 6.